JACS
JOURNAL OF THE AMERICAN CHEMICAL SOCIETY
Communication
pubs.acs.org/JACS

A Single-Molecule Magnet Based on Heptacyanomolybdate with the Highest Energy Barrier for a Cyanide Compound

Kun Qian,[†] Xing-Cai Huang,[†] Chun Zhou,[†] Xiao-Zeng You,[†] Xin-Yi Wang,*[,†] and Kim R. Dunbar*[,‡]

[†]State Key Laboratory of Coordination Chemistry, School of Chemistry and Chemical Engineering, Nanjing University, Nanjing 210093, China

[‡]Department of Chemistry, Texas A&M University, College Station, Texas 77840, United States

Supporting Information

ABSTRACT: Three trinuclear Mn_2Mo molecules based on the orbitally degenerate $[Mo(CN)_7]^{4-}$ anion were prepared, one of which is the first single-molecule magnet (SMM) based on heptacyanomolybdate. The blocking temperature and the energy barrier (U = 40.5 cm^{-1}) are records for a cyanide-based SMM. Wide hysteresis loops and sharp quantum tunneling steps were observed from single-crystal measurements.

The discovery of magnetic bistability in the mixed-valence $Mn_4^{IV}Mn_8^{III}$ dodecanuclear compound $Mn_{12}O_{12}(O_2CCH_3)_{16}(H_2O)_4$, commonly referred to as Mn_{12}-acetate, launched an entirely new field of study focusing on the fascinating intermediate regime between the realms of paramagnetism and bulk magnetism.[1] Single-molecule magnets (SMMs) are fundamentally different from traditional magnetic materials in that slow magnetic relaxation and magnetic hysteresis are entirely molecular in origin. Moreover, their nonclassical behavior, including quantum tunneling of the magnetization (QTM)[2] and quantum phase interference,[3] opens up the potential for using SMMs in spintronic devices and quantum computing.[4] Progress in the field notwithstanding, the magnetization reversal barriers (U) and blocking temperatures (T_B) for SMMs remain relatively low. The energy barrier for the majority of SMMs is related to the molecular ground state spin S and zero-field splitting (ZFS) parameter D, which is $U = S^2|D|$ or $(S^2 - 1/4)|D|$ for integer and half-integer spin, respectively (with a ZFS Hamiltonian $H = D[S_z^2 - S(S + 1)/3]$).[1] Although it is obvious that, hypothetically, one can raise the barrier by increasing the values of S and D, in practice, large S and D values are countervailing trends.[5,6] Consequently, in spite of the discovery of numerous SMMs, some with very large nuclearities and S values,[7,8] the record energy barriers were held by the Mn_{12} family of molecules for a decade until the report of a Mn_6 compound in 2007.[9]

Recently, it has become increasingly obvious that high magnetic anisotropy is the most critical requirement for an SMM, and, in this vein, metal ions with unquenched orbital angular momentum including 3d metal ions with certain oxidation states and geometries,[10,11] f-block elements,[12−15] and 4d and 5d metal ions with strong spin−orbit coupling and strong anisotropic magnetic exchange[16−18] have been targeted. Indeed, research in the area of lanthanide metal-based SMMs has led to exciting findings for which the U_{eff} (effective energy barrier) and T_B values are as high as 600 cm^{-1} and 14 K, respectively.[13,14] In addition, SMMs with actinide elements are also very attractive targets, with interesting magnetic properties being reported.[15]

Recent work in our laboratories has focused on the $[Mo^{III}(CN)_7]^{4-}$ anion, which is of particular interest given the theoretical prediction that $[Mo^{III}(CN)_7]^{4-}$ will lead to high T_B SMMs due to strong anisotropic magnetic exchange,[19] a hypothesis that have been awaiting experimental verification for a decade. In fact, compounds of $[Mo^{III}(CN)_7]^{4-}$ anion remain quite scarce in general, presumably because of its sensitivity, high negative charge, and numerous binding modes. Early pioneering work with heptacyanomolybdate by the Kahn group in the 1990s, as well as subsequent studies by several other researchers, produced interesting 2-D and 3-D magnets, including a recent finding of two 3-D phases that undergo a crystal-to-crystal transformation with dramatic changes in magnetic ordering by the Dunbar group.[20−24] Of particular relevance to the current topic is our recent report on the only molecular compound of $[Mo^{III}(CN)_7]^{4-}$, namely a molecule based on the docasanuclear $Mn^{II}_{14}Mo^{III}_8$ unit with an S = 31 ground state which engages in strong intermolecular dipole interactions that suppress SMM behavior.[25]

Herein we present the syntheses, structures, and magnetic properties of three structurally related $Mn^{II}_2Mo^{III}$ compounds, $[Mn(L_{N_5Me})(H_2O)]_2[Mo(CN)_7]\cdot 6H_2O$ (**1**), $[Mn(L_{N_3O_2})(H_2O)]_2[Mo(CN)_7]\cdot 7H_2O$ (**2**), and $[Mn(L_{DAPSC})(H_2O)]_2[Mo(CN)_7]\cdot 6H_2O\cdot CH_3CN$ (**3**) (see Figure 1a for the ligands L_{N_5Me}, $L_{N_3O_2}$, and L_{DAPSC}). Notably, despite the rather small S = 9/2 ground spin state, the barrier U_{eff} of the trinuclear complex **1** rivals that of the seminal Mn_{12}-acetate compound with S = 10 and represents the highest for a cyanide-based SMM reported thus far. Hysteresis loops and sharp quantum tunneling steps were observed at up to 3.2 K. The two other Mn_2Mo isomers, compounds **2** and **3**, exhibit only simple paramagnetic behavior.

Syntheses of **1**−**3** were achieved by using three similar pentadentate capping ligands for the Mn^{II} centers with careful adjustment of the reaction conditions (Supporting Information). Structures of **1**−**3** were determined by single-crystal X-ray diffraction studies and found to be $Mn^{II}_2Mo^{III}$ trinuclear complexes with two Mn^{II} capping groups and one Mo^{III} ion

Received: July 3, 2013
Published: August 22, 2013

   dx.doi.org/10.1021/ja4067833 | J. Am. Chem. Soc. 2013, 135, 13302−13305

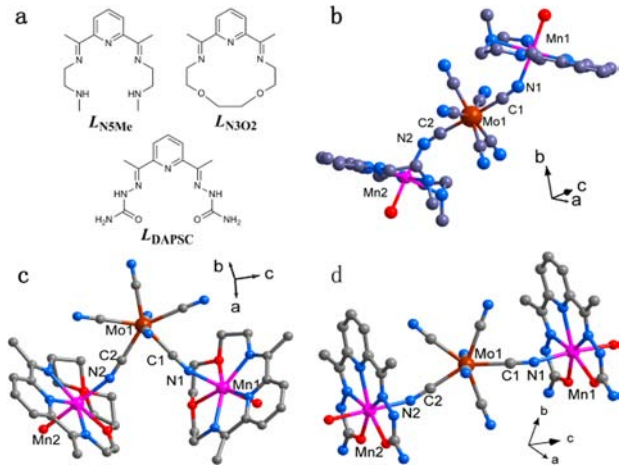

Figure 1. (a) Structures of the three pentadentate ligands: L_{N_5Me}, $L_{N_3O_2}$, L_{DAPSC}. (b–d) Structures of the trinuclear $Mn^{II}_2Mo^{III}$ compounds of **1** (b), **2** (c), and **3** (d).

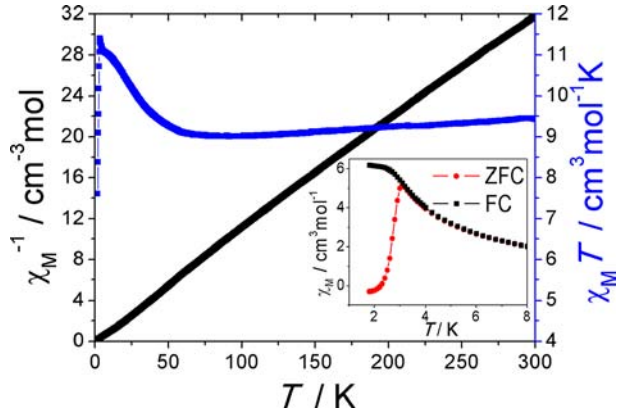

Figure 2. Temperature-dependent magnetic susceptibility of **1** measured at 1 kOe. Inset: ZFC and FC data measured under 5 Oe with a temperature sweep rate of 2 K/min.

connected via two CN^- groups (Figure 1b–d). Apart from small changes in bond distances and angles involving the metal centers (Table S2), the primary difference is the relative positions of the two Mn^{II} units on the pentagonal bipyramid of $[Mo(CN)_7]^{4-}$. In **1**, the two Mn^{II} units are bound to the Mo^{III} ion through the two axial CN^- groups, whereas in **2** and **3** they are connected to the equatorial CN^- groups, specifically in *ortho*-1,2 and *meta*-1,3 positions for **2** and **3**, respectively. The $[Mo(CN)_7]^{4-}$ anion in all three complexes is only slightly distorted from the ideal D_{5h} geometry, which is magnetically important since the deviation from the D_{5h} geometry is predicted to reduce the magnetic anisotropy of the Mo^{III} center.[19] The Mn^{II} ions in **1**–**3** are in a pentagonal bipyramidal environment with seven coordinate atoms, five of which are from the macrocyclic ligand, with the remaining two being a nitrogen atom from a bridging CN^- and an oxygen atom from a coordinated water. The Mo–C–N bond angles in the Mo–C–N–Mn linkage are all close to linear, whereas the C–N–Mn bond angles are significantly bent, being 145.7(3) and 149.5(3)° for **1**, 152.3(3) and 161.7(3)° for **2**, and 154.0(3) and 156.7(3)° for **3**, respectively. For **1**, every Mn_2Mo unit is connected to four nearest neighbors by hydrogen bonds between the coordinated water molecules (O1 and O2) and nitrogen atoms from the $[Mo(CN)_7]^{4-}$ unit (O1···N5 = 2.88 and O2···N3 = 2.99 Å) (Figure S1). In addition, numerous hydrogen bonds involving the uncoordinated water molecules for all three compounds are evident in the structures (Figures S2–S4).

Direct current (dc) magnetic susceptibilities were measured on polycrystalline samples of **1**–**3** over the temperature range 1.8–300 K at a dc field of 1 kOe. For **2** and **3**, the $\chi_M T$ versus T plots show a continuous decrease upon cooling, owing to dominant antiferromagnetic interactions between the Mo^{III} and Mn^{II} centers (Figures S5 and S6). Importantly, the alternating current (ac) susceptibilities of **2** and **3** measured under a zero dc field show no appearance of out-of-phase signals (Figures S7 and S8), ruling out SMM behavior. In the case of the data for **1**, the $\chi_M T$ value decreases from 9.42 cm^3 mol^{-1} K at 300 K to a minimum of 9.00 cm^3 mol^{-1} K at 85 K and then increases slowly to a maximum of 11.4 cm^3 mol^{-1} K at 3.5 K and finally decreases again down to 2 K (Figure 2). Whereas there are no abnormalities in the $\chi_M T$ versus T curves for **2** and **3**, a small peak at ∼3 K for **1** indicates magnetic blocking, which was confirmed by the sharp divergence at 3.1 K in the field-cooled (FC) and zero-field-cooled (ZFC) magnetic susceptibility data measured under a 5 Oe dc field with a temperature sweep rate of 2 K/min (Figure 2 inset).

To probe the SMM property of **1**, the temperature- and frequency-dependent ac susceptibility data were collected under a zero dc field (Figures 3 and S9). A pronounced frequency dependence was observed with a shift parameter $\phi = (\Delta T_p/T_p)/\Delta(\log f) = 0.15$ (where T_p represents the peak temperatures in in-phase χ_M' plots and f is the frequency of the ac field), which is in the normal range for a SMM and considerably greater than that for a spin glass.[26] The Cole–Cole plots (Figure S10) of **1** at temperatures from 4.0 to 7.0 K exhibit a symmetric shape and can be fitted to the generalized Debye model, with α parameters below 0.20 (Table S3), indicating a narrow distribution of relaxation times.[27] The dc magnetization decay was monitored in the range 1.8–2.8 K, at temperatures where the magnetic relaxation is too slow to be measured by the ac method (Figure S11). At temperatures above 2.3 K, the magnetization decay can be fitted well with a single-exponential decay, but below 2.2 K, the relaxation profile is best described by a stretched exponential decay ($M = M_0 \exp(-(t/\tau)^B)$; $\ln(M) = \ln(M_0) - (t/\tau)^B$) (Figure S12 and Table S4), suggesting that the magnetic decay is initially fast and then becomes slower with time.[28] The magnetic relaxation time (τ) as a function of $1/T$ derived from both the ac and dc measurements, as plotted in Figure 3c, shows a thermally activated process and can be fitted to an Arrhenius law $\tau = \tau_0 \exp(U_{eff}/k_BT)$, with $U_{eff} = 40.5 \pm 0.3$ cm^{-1} (58.5 ± 0.4 K) and an attempting time $\tau_0 = (2.0 \pm 0.3) \times 10^{-8}$ s ($R^2 = 0.998$). The relaxation time at 1.8 K is estimated to be 2.73×10^6 s, which is approximately 1 month. Although the energy barrier is lower than those of many 4f-based SMMs,[12] it constitutes a new record among cyanide-bridged SMMs, with the previously reported largest barrier being 33 cm^{-1} for a Mn_4Re compound.[18]

The SMM behavior of **1** was further confirmed by the observation of hysteresis loops. As depicted in Figures 4, S13, and S14, highly distinct hysteresis loops were observed for both powders and a single crystal (of mass = 0.46 mg) from 1.8 to 3.2 K and field sweep rates of 0.01–0.05 T/s. For the single crystal, the loops were measured without orientation as well as with orientation along the crystal easy-axis by applying a 5 T

dx.doi.org/10.1021/ja4067833 | J. Am. Chem. Soc. 2013, 135, 13302–13305

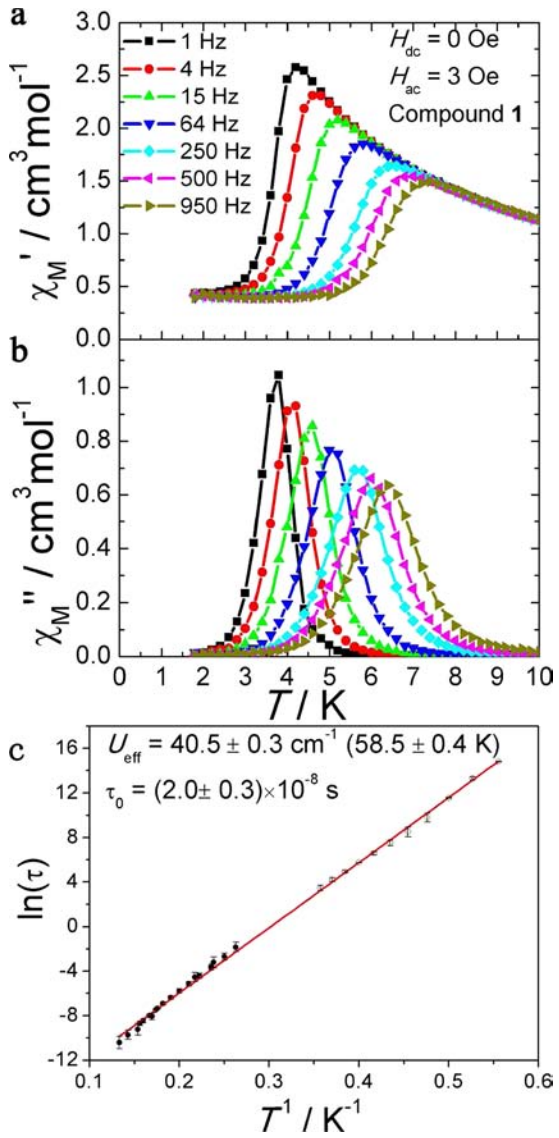

Figure 3. Temperature-dependent in-phase (a) and out-of-phase (b) ac susceptibilities for **1** under H_{ac} = 2 Oe and H_{dc} = 0 Oe. (c) Relaxation time fit to the Arrhenius law for **1**. Open circles represent data derived from ac measurements, and filled circles represent data from dc magnetization decay measurements.

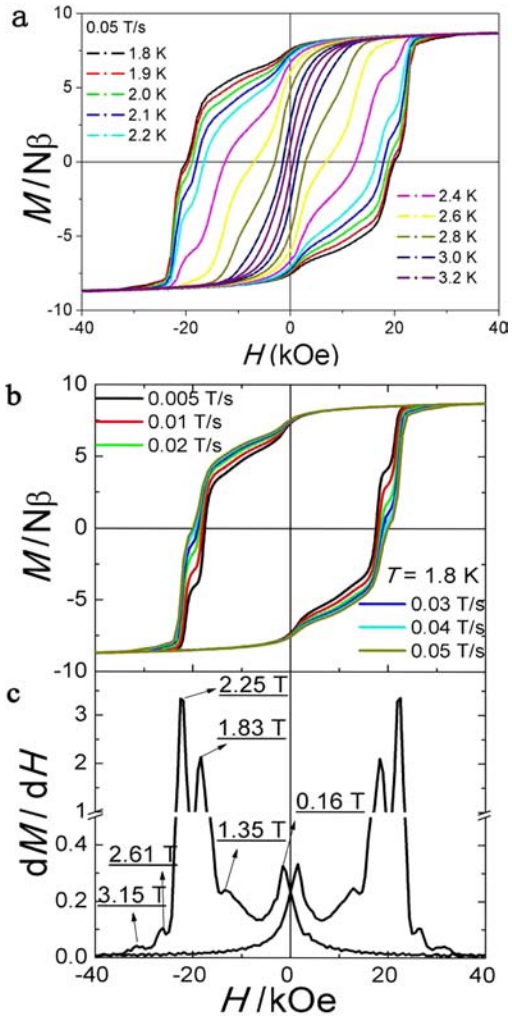

Figure 4. (a,b) Temperature- and field sweep rate-dependent magnetic hysteresis loops for a single crystal of **1** measured at the indicated conditions. (c) Derivative of the magnetization (dM/dH) versus magnetic field for the curves measured at 1.8 K at a sweep rate of 0.03 T/s.

magnetic field on the crystal embedded in eicosane. The loop remains open until ∼3.2 K (Figure 4a), at which temperature the relaxation time is estimated to be 2 s. For the loops collected on both the unoriented single crystal and powders, the remnant magnetization at zero field and the largest magnetization at 7 T are significantly lower than the values for the oriented single crystal, indicating strong magnetic anisotropy in **1**. For the oriented single crystal, the magnetization nearly saturates at fields larger than 1 T and reaches 9.0 μ_B at 7 T, suggesting a 9/2 ground state of **1** assuming $g \approx 2$. The coercivities of the loops are as large as 2.0 T at 1.8 K and a field sweep rate of 0.05 T/s and become larger with decreasing temperature and increasing field sweep rate, as expected for SMMs. Moreover, the loops exhibit obvious step-like features, corresponding to resonant quantum tunneling between opposite spin states.[2] The critical fields H_n for the QTM corresponding to these steps were estimated from the dM/dH curves as depicted in Figure 4c. Apart from the large coercivities exhibited by **1**, the main observation that warrants emphasis is that the critical fields H_n for the QTM of **1** are irregularly spaced, which is strikingly different from the existing SMMs in the literature. For a typical SMM with a parabolic energy barrier of $U = |D|S^2$, the QTM normally occurs at a constant interval of field ($\Delta H = D/(g\mu_B)$), provided the ground state is isolated and only the axial ZFS term need be considered.[1,2]

The only origin of the magnetic anisotropy and SMM behavior of **1** is the $[Mo(CN)_7]^{4-}$ unit, given that the 3d^5 Mn^{II} center possesses an isotropic $^6A_1$ ground state with a very small ZFS energy, as confirmed by the small D value (approximately −0.07 cm^{-1}) of the starting material $Mn(L_{N_5Me})Cl_2 \cdot 1/2H_2O \cdot 3/4CH_3OH$, estimated from the fitting of the reduced magnetization data (Figure S15). The strong single-ion magnetic anisotropy of $[Mo(CN)_7]^{4-}$ can manifest itself only in a highly anisotropic g-tensor but not in terms of ZFS, given that the anion contains a low-spin (S = 1/2) Mo^{III} center. The fact that compounds **2** and **3** behave as simple paramagnets above 1.8 K implies that the SMM behavior of **1** originates from the magnetic exchange coupling between the Mo^{III} and Mn^{II} centers, which can be very anisotropic and is closely related to the positions of the CN$^-$ groups in the pentagonal bipyramid

dx.doi.org/10.1021/ja4067833 | J. Am. Chem. Soc. 2013, 135, 13302−13305

geometry, as predicted in the previously described theoretical model.[19] According to this model, the exchange interaction for the linear apical Mo^{III}−CN−Mn^{II} pairs can be described by an Ising-like spin Hamiltonian $JS^z_{Mo}S^z_{Mn}$, which represents a very important source of the required magnetic anisotropy for a SMM. Furthermore, the energy diagram of the low-lying states for the resulting SMM will be significantly different from the well-known double-well potential diagram, for which the ground state S is split by the easy-axis ZFS ($|D_z|S_z^2$). This situation leads to irregular intervals in the critical fields for the QTM observed for **1**.

In summary, the first $[Mo(CN)_7]^{4-}$-based single-molecule magnet has been synthesized and fully characterized. The SMM characteristics of **1** are comparable to those of the seminal Mn_{12}-acetate compound despite the fact that the molecule exists in an $S = 9/2$ ground state as compared to $S = 10$ for Mn_{12}. These results constitute an important finding in terms of the promise for obtaining higher blocking temperature cyanide SMMs than what has been previously thought to be possible, given the rather modest results thus far obtained with 3d hexacyanometallates. Exploration of additional experimental details and theoretical analyses are in progress to fully understand the origin of the unusual magnetic properties for the axial molecule and the lack of SMM behavior for the equatorial isomers.

■ ASSOCIATED CONTENT

Supporting Information

X-ray crystallographic files in CIF format, experimental details, crystallographic data, and additional structural and magnetic figures and tables. This material is available free of charge via the Internet at http://pubs.acs.org.

■ AUTHOR INFORMATION

Corresponding Author

wangxy66@nju.edu.cn; dunbar@mail.chem.tamu.edu

Notes

The authors declare no competing financial interest.

■ ACKNOWLEDGMENTS

X.-Y.W. thanks the Major State Basic Research Development Program (2013CB922102), NSFC (91022031, 21021062, 21101093) and the NSF of Jiangsu province (BK2011548) for financial assistance. The synthetic work by X.-Y.W. while he was a Postdoctoral Research Associate in the Dunbar laboratories was supported by the U.S. Department of Energy (DE-FG02-02ER45999).

■ REFERENCES

(1) (a) Gatteschi, D.; Sessoli, R. *Angew. Chem., Int. Ed.* **2003**, *42*, 268−297. (b) Gatteschi, D.; Sessoli, R.; Villain, J. *Molecular Nanomagnets*; Oxford University Press: Oxford, UK, 2006.

(2) (a) Thomas, L.; Lionti, F.; Ballou, R.; Gatteschi, D.; Sessoli, R.; Barbara, B. *Nature* **1996**, *383*, 145−147. (b) Friedman, J. R.; Sarachik, M. P.; Tejada, J.; Ziolo, R. *Phys. Rev. Lett.* **1996**, *76*, 3830−3833. (c) Wernsdorfer, W.; Aliaga-Alcalde, N.; Hendrickson, D. N.; Christou, G. *Nature* **2002**, *416*, 406−408.

(3) (a) Wernsdorfer, W.; Sessoli, R. *Science* **1999**, *284*, 133−135. (b) Hill, S.; Edwards, R. S.; Aliaga-Alcalde, N.; Christou, G. *Science* **2003**, *302*, 1015−1018.

(4) (a) Leuenberger, M. N.; Loss, D. *Nature* **2001**, *410*, 789−793. (b) Ardavan, A.; Rival, O.; Morton, J. J. L.; Blundell, S. J.; Tyryshkin, A. M.; Timco, G. A.; Winpenny, R. E. P. *Phys. Rev. Lett.* **2007**, *98*, 057201. (c) Bogani, L.; Wernsdorfer, W. *Nat. Mater.* **2008**, *7*, 179−186. (d) Troiani, F.; Affronte, M. *Chem. Soc. Rev.* **2011**, *40*, 3119−3129.

(5) Oshio, H.; Nakano, M. *Chem.—Eur. J.* **2005**, *11*, 5178−5185.

(6) (a) Waldmann, O. *Inorg. Chem.* **2007**, *46*, 10035−10037. (b) Ruiz, E.; Cirera, J.; Cano, J.; Alvarez, S.; Loose, C.; Kortus, J. *Chem. Commun.* **2008**, 52−54. (c) Neese, F.; Pantazis, D. A. *Faraday Discuss.* **2011**, *148*, 229−238.

(7) Tasiopoulos, A. J.; Vinslava, A.; Wernsdorfer, W.; Abboud, K. A.; Christou, G. *Angew. Chem., Int. Ed.* **2004**, *43*, 2117−2121.

(8) Ako, A. M.; Hewitt, I. J.; Mereacre, V.; Clérac, R.; Wernsdorfer, W.; Anson, C. E.; Powell, A. K. *Angew. Chem., Int. Ed.* **2006**, *45*, 4926−4929.

(9) Milios, C. J.; Vinslava, A.; Wernsdorfer, W.; Moggach, S.; Parsons, S.; Perlepes, S. P.; Christou, G.; Brechin, E. K. *J. Am. Chem. Soc.* **2007**, *129*, 2754−2755.

(10) Zadrozny, J. M.; Xiao, D. J.; Atanasov, M.; Long, G. J.; Grandjean, F.; Neese, F.; Long, J. R. *Nature Chem.* **2013**, *5*, 577−581.

(11) Vallejo, J.; Castro, I.; Ruiz-García, R.; Cano, J.; Julve, M.; Lloret, F.; Munno, G.; Wernsdorfer, W.; Pardo, E. *J. Am. Chem. Soc.* **2012**, *134*, 15704−15707.

(12) (a) Woodruff, D. N.; Winpenny, R. E. P.; Layfield, R. A. *Chem. Rev.* **2013**, *113*, 5110−5148. (b) Sessoli, R.; Powell, A. K. *Coord. Chem. Rev.* **2009**, *253*, 2328. (c) Rinehart, J. D.; Long, J. R. *Chem. Sci.* **2011**, *2*, 2078−2085.

(13) Gonidec, M.; Biagi, R.; Corradini, V.; Moro, F.; De Renzi, V.; Pennino, I.; Summa, D.; Muccioli, L.; Zannoni, C.; Amabilino, D. B.; Veciana, J. *J. Am. Chem. Soc.* **2011**, *133*, 6603−6612.

(14) (a) Rinehart, J. D.; Fang, M.; Evans, W. J.; Long, J. R. *Nature Chem.* **2011**, *3*, 538−542. (b) Rinehart, J. D.; Fang, M.; Evans, W. J.; Long, J. R. *J. Am. Chem. Soc.* **2011**, *133*, 14236−14239.

(15) (a) Mills, D. P.; Moro, F.; McMaster, J.; Slageren, J.; Lewis, W.; Blake, A. J.; Liddle, S. T. *Nature Chem.* **2011**, *3*, 454−460. (b) Mougel, V.; Chatelain, L.; Pécaut, J.; Caciuffo, R.; Colineau, E.; Griveau, J. C.; Mazzanti, M. *Nature Chem.* **2012**, *4*, 1011−1017.

(16) Wang, X. Y.; Avendaño, C.; Dunbar, K. R. *Chem. Soc. Rev.* **2011**, *40*, 3213−3238 and references therein.

(17) (a) Dreiser, J.; Pedersen, K. S.; Schnegg, A.; Holldack, K.; Nehrkorn, J.; Sigrist, M.; Tregenna-Piggott, P.; Mutka, H.; Weihe, H.; Mironov, V. S.; Bendix, J.; Waldmann, O. *Chem.—Eur. J.* **2013**, *19*, 3693−3701. (b) Pedersen, K. S.; Dreiser, J.; Nehrkorn, J.; Gysler, M.; Schau-Magnussen, M.; Schnegg, A.; Holldack, K.; Bittl, R.; Piligkos, S.; Weihe, H.; Tregenna-Piggott, P.; Waldmann, O.; Bendix, J. *Chem. Commun.* **2011**, *47*, 6918−6920.

(18) Freedman, D. E.; Jenkins, D. M.; Iavarone, A. T.; Long, J. R. *J. Am. Chem. Soc.* **2008**, *130*, 2884−2885.

(19) (a) Mironov, V. S.; Chibotaru, L. F.; Ceulemans, A. *J. Am. Chem. Soc.* **2003**, *125*, 9750−9760. (b) Mironov, V. S. *Dokl. Phys. Chem.* **2006**, *408*, 130−136.

(20) Kahn, O.; Larionova, J.; Ouahab, L. *Chem. Commun.* **1999**, 945−952.

(21) Le Goff, X. F.; Willemin, S.; Coulon, C.; Larionova, J.; Donnadieu, B.; Clérac, R. *Inorg. Chem.* **2004**, *43*, 4784−4786.

(22) Milon, J.; Daniel, M. C.; Kaiba, A.; Guionneau, P.; Brandès, S.; Sutter, J. P. *J. Am. Chem. Soc.* **2007**, *129*, 12872−12878.

(23) Tomono, K.; Tsunobuchi, Y.; Nakabayashi, K.; Ohkoshi, S. *Inorg. Chem.* **2010**, *49*, 1298.

(24) Wang, Q. L.; Southerland, H.; Li, J. R.; Prosvirin, A. V.; Zhao, H.; Dunbar, K. R. *Angew. Chem., Int. Ed.* **2012**, *51*, 9321−9324.

(25) Wang, X. Y.; Prosvirin, A. V.; Dunbar, K. R. *Angew. Chem., Int. Ed.* **2010**, *49*, 5081−5084.

(26) Mydosh, J. A. *Spin Glasses: an Experimental Introduction*; Taylor & Francis: London, 1993.

(27) Cole, K. S.; Cole, R. H. *J. Chem. Phys.* **1941**, *9*, 341−352.

(28) Aubin, S. M.; Dilley, N. R.; Pardi, L.; Krzystek, J.; Wemple, M. W.; Brunel, L. C.; Maple, M. B.; Christou, G.; Hendrickson, D. N. *J. Am. Chem. Soc.* **1998**, *120*, 4991−5004.